

Short-term plasticity constrains spatial organization of a hippocampal presynaptic terminal

Suhita Nadkarni^{a,b}, Thomas M. Bartol^{a,b}, Charles F. Stevens^b, Terrence J. Sejnowski^{a,b,c}, and Herbert Levine^{a,1}

^aCenter for Theoretical Biological Physics, University of California at San Diego, La Jolla, CA 92093; ^bSalk Institute for Biological Studies, La Jolla, CA 92037; and ^cHoward Hughes Medical Institute, Salk Institute for Biological Studies, La Jolla, CA 92037

Contributed by Herbert Levine, July 25, 2012 (sent for review April 24, 2012)

Although the CA3–CA1 synapse is critically important for learning and memory, experimental limitations have to date prevented direct determination of the structural features that determine the response plasticity. Specifically, the local calcium influx responsible for vesicular release and short-term synaptic facilitation strongly depends on the distance between the voltage-dependent calcium channels (VDCCs) and the presynaptic active zone. Estimates for this distance range over two orders of magnitude. Here, we use a biophysically detailed computational model of the presynaptic bouton and demonstrate that available experimental data provide sufficient constraints to uniquely reconstruct the presynaptic architecture. We predict that for a typical CA3–CA1 synapse, there are ~70 VDCCs located 300 nm from the active zone. This result is surprising, because structural studies on other synapses in the hippocampus report much tighter spatial coupling. We demonstrate that the unusual structure of this synapse reflects its functional role in short-term plasticity (STP).

synaptic depression | paired-pulse facilitation | vesicle | MCcell

Synaptic transmission is determined by the local calcium signal detected at the active zone, the actual locus of neurotransmitter release (1–3). Current experimental techniques can only measure the global calcium signal in a synaptic bouton. However, diffusion of calcium between its sources and sinks at the active zone, means that the local calcium concentration may be very different from the averaged global concentration. This concentration is transient and determined by the number of presynaptic voltage-dependent calcium channels (VDCCs), the main source of calcium, the distance between them and the active zone, and the calcium buffers and pumps in the terminal, the main sinks of calcium. The spatiotemporal properties of this calcium signal finely orchestrate many aspects of synaptic plasticity; hence these depend critically on the architectural features. Here we describe a unique computational approach that uses measurable quantities as modeling constraints and thus can compensate for the lack of direct structural evidence. In this manner, the model answers a key question in synaptic neurophysiology, namely, what is the number and geometry of the calcium channels at the CA3–CA1 synapse, crucial in learning and memory.

Pharmacological and electrophysiological experiments at different synapses have reached different conclusions regarding presynaptic architecture. The frog neuromuscular junction, mouse hair cell ribbon synapse, and squid giant synapse all require only a small number of channels placed close to the release sites for vesicle fusion (4–8). In contrast, tens of channels are said to control fusion in the calyx of Held and cerebellar synapses (9–11). For small GABAergic synapses in the hippocampus, recent studies (12, 13) show that calcium channels and the active zone share a tight geometrical arrangement. This feature is argued to be essential for fast, efficient, and reliable synapses (13). For the CA3–CA1 synapse in the hippocampus, where plasticity, more than reliability, is likely to be the most valued attribute, the exact number of VDCCs and separation distance, l_c , from the active zone (and how these structural details affect function) is unknown.

The finer details of the CA3–CA1 hippocampal synapse are largely inaccessible to existing experimental techniques. However,

existing experimental data provide sufficiently overlapping constraints to develop computational approaches that can reliably infer these details. In general the use of models as a “computational microscope” in direct conjunction with data is an extremely powerful approach (14–16). In particular, we demonstrate here that the relationship between the active zone and VDCCs in the CA3–CA1 synapse in the hippocampus is spatially extended, which is the exact opposite of what could have been expected on the basis of the aforementioned results for small GABAergic synapses.

The CA3–CA1 synapse is a well-studied prototype for plasticity. Our structural results have direct consequences for short-term plasticity (STP). At a tightly coupled synapse where the VDCCs are close to the calcium sensor, only a few channels are needed to raise the local calcium levels sufficiently to cause release. Such a local event would have minimal impact on the global calcium levels. Conversely, at a synapse where the VDCCs are at distant sites from the calcium sensor, activation of a large number would be needed to trigger release and would result in an augmented calcium level in the entire terminal. The latter is what we have found for the CA3–CA1 case. The elevation of the global calcium concentration has important consequences for the facilitation of the response to a subsequent stimulus, because residual (bound and free) calcium can enhance the release probability (2, 17). Our realistic model makes testable predictions for paired-pulse facilitation (PPF) and for other plasticity protocols that will further constrain dynamic models of neural circuits.

Results

Quantifying the Local Calcium Signal at the Active Zone. Several laboratories have focused on determining the average baseline probability of neurotransmitter release (18) and the global calcium response due to arrival of an action potential in the terminal (19). However, it is the local calcium signal at the active zone that dictates the neurotransmitter release probability at a given synapse and this is much more difficult to determine.

In a previous study, we modeled vesicle release at the CA3–CA1 synapse; this model was stringently matched to release data from several independent laboratories (14). There is an excellent match between the decay timescales of neurotransmitter release transients and maximum amplitudes of the release transients in the model (14), and that measured at the CA3–CA1 synapse (20). Furthermore the calcium sensitivity of the model agrees with that measured in the calyx of Held synapse; this is to be expected because fast transmission at both these synapses has a similar profile and is governed by either Synaptotagmin I or Synaptotagmin II (14, 21, 22). The kinetic characteristics of Synaptotagmin I are close to those of Synaptotagmin II, with Synaptotagmin I slightly faster (14, 23, 24). This model also

Author contributions: S.N., T.M.B., C.F.S., T.J.S., and H.L. performed research; and S.N., T.M.B., T.J.S., and H.L. wrote the paper.

The authors declare no conflict of interest.

Freely available online through the PNAS open access option.

¹To whom correspondence should be addressed. E-mail: hlevine@ucsd.edu.

This article contains supporting information online at [www.pnas.org/lookup/suppl/doi:10.1073/pnas.1211971109/-DCSupplemental](http://www.pnas.org/lookup/suppl/doi:10.1073/pnas.12119711109/-DCSupplemental).

accurately predicted the spontaneous activity rate per bouton and the readily releasable pool (RRP) size at the CA3–CA1 synapse.

We use this framework to show how structural properties of the synapse and the local calcium signal at the active zone may be inferred from measurable features. Fig. S1 shows a typical release event from the model.

In Fig. 1A we show the predicted peak of the *global* calcium transient (total number of calcium ions) in the presynaptic terminal as a function of l_c and VDCC number. The l_c range (25–400 nm) and the VDCC number (1–200) simulated here cover the possible ranges associated with a single active zone. The contour lines indicate intrinsic values of the neurotransmitter release probability, p_{r1} (release probability in response to the first stimulus) associated with a synapse with an ultrastructure by the given VDCC number (y axis) and l_c (x axis). It is therefore clear that a synapse can achieve a specific release probability by either having a small number of channels very close to the calcium sensor (small l_c) or a large number of VDCCs far away (large l_c). Thus, the release is strongly correlated with the local calcium signal, characterized by either its peak value (Fig. 1B) or its integrated strength (Fig. 1C, full width at half maximum, FWHM). Conversely, the global calcium depends weakly on the geometrical factors and mostly reflects VDCC number. Thus, using two synaptic “measurables,” the global calcium response and the base-level release probability, p_{r1} , we can infer unique values for both VDCC number and l_c .

It is worth noting that neurotransmitter release is completely governed by the calcium profile that the sensor sees and the peak of this local calcium transient is typically used to characterize its calcium sensitivity. However, synapses with equal release probabilities can have differing calcium profiles (Fig. 1B and C); VDCCs placed further away give rise to a shorter and broader local calcium peak (a more diffuse signal) compared with VDCCs placed closer (Fig. S2). Thus, there is a set of calcium sensitivity profiles rather than a unique curve.

Predicting the VDCC Number Using Fluctuation Analysis. In the previous section we described a method to determine synaptic organization that relies directly on knowing the kinetic rates of the calcium sensor for neurotransmitter release. It would be desirable

to have a complementary approach that could estimate structural parameters in a kinetics-model-independent manner. This is in fact possible because the leading contribution to the spike-to-spike variability in the global calcium signal comes from the stochastic openings and closings of the VDCCs (25). Hence measuring this variance can be used to directly determine the number of channels.

To study this in more detail, we modified the simulations by allowing the flux from each channel to be an independent variable, such that each channel cluster (consisting of 1–200 channels) can generate the complete range of mean calcium profiles. In Fig. 2A, we show a plot of coefficient of variation (CV) of global calcium response in the presynaptic terminal, calculated by running 1,000 trials, predicted by the model. By measuring the CV of the global calcium response, it is possible to uniquely determine the VDCC number. Fluorescent calcium indicators are used to quantify calcium responses. In Fig. 2B, the simulations included fluo-4FF, a fluorescent calcium dye well calibrated for in vitro experiments at the level of the synapse. As expected, the CV of the fluorescence reflected the fluctuation attributes of different VDCC numbers as seen in Fig. 2A. This fluctuation analysis is robust and independent of channel type, placement of the channel, and details of the calcium sensor for neurotransmitter release.

For illustration in Fig. 2C and D we show the bound calcium dye (fluo-4FF) for four different stochastic trials when the source of calcium is a single channel (Fig. 2C) or 200 (Fig. 2D) channels, respectively. These data illustrate the high level of fluctuations, due to normal stochastic opening and closing of calcium channels, when the channel number is low. Conversely, when there is a large number of channels there is less variability in the peak response.

Predicting l_c Using Release Delays. Diffusion of calcium in the presynaptic terminal is not free but instead is limited by molecules that can bind calcium, which mainly include buffers and pumps. Intracellular calcium therefore appears to diffuse more slowly at $\sim 50 \mu\text{m}^2/\text{s}$ compared with its cytoplasmic, free diffusion constant of $\sim 200 \mu\text{m}^2/\text{s}$ (Fig. S3A and B). Following the opening of VDCCs and entry of calcium in the terminal, calcium ions diffuse from the source (VDCCs), through the gauntlet of calcium-binding proteins, to the active zone and subsequently bind to the calcium sensor before a vesicle can be released. This

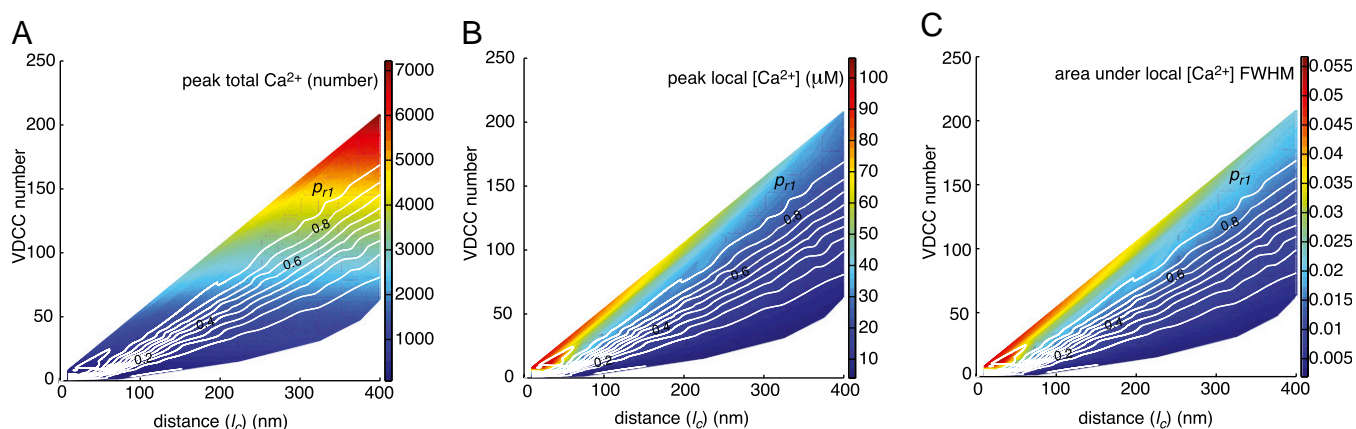


Fig. 1. Predicting the presynaptic structure from global calcium response and vesicle release probability. (A) Peak of the total calcium signal in the terminal (color plot) as a result of opening of VDCCs is shown as a function of VDCC number and l_c . Release probabilities (white contour lines) for each combination of VDCC number and l_c are superimposed on global calcium data. The range of VDCC numbers and l_c described here spans the parameter space for all possible physiological values. (B) Peak of the local calcium profile (color plot) measured 10 nm from the calcium sensor is shown as a function of VDCC number and l_c . Because it is not possible to probe the local calcium signal directly, one can use the information acquired on VDCC number and l_c using Fig. 1A to estimate the local calcium profile from this figure. Release probability contours (white lines) do not follow the color gradient accurately because the shape of the local calcium profile changes with l_c (Fig. S2). (C) Area under the full width at half maximum (FWHM) of the local calcium signal (color plot) is shown as VDCC number and l_c is varied. FWHM is a better indicator of calcium sensitivity of the sensor. Fig. 1C and B gives a better description of the local calcium signal than just the peak of the calcium signal alone.

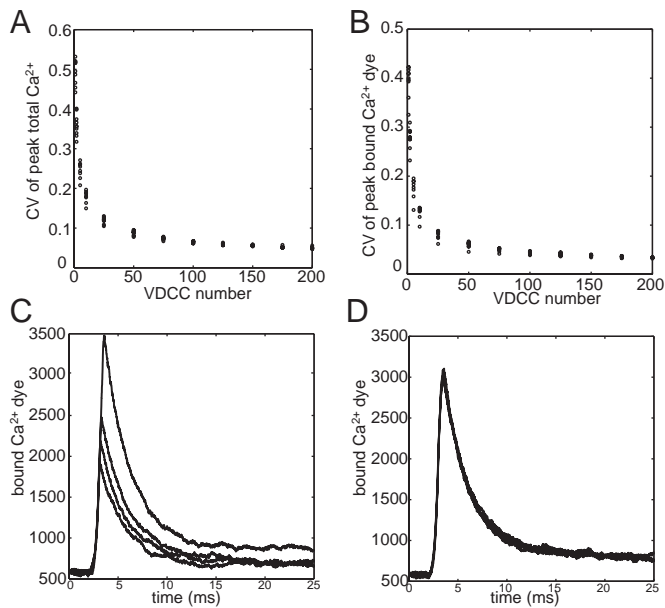


Fig. 2. Using fluctuation analysis to predict VDCC number. (A) Coefficient of variance (CV) over 1,000 trials (each dot) of the total calcium response as a function of VDCC number. The flux of calcium coming through each channel was varied (fraction of micromoles to tens of micromoles) to cover the entire range of release probabilities for a given number of channels. The series of dots for each VDCC number represents various release probabilities, p_{r1} , (lower p_{r1} , implying lower incoming calcium flux, leads to larger CV). (B) Simulations with fluo-4FF calcium dye and the CV of the fluorescence at the peak of the calcium response as a function of VDCC number. (C) Representative trials exhibited a highly variable dye response with one VDCC and (D) low variability with 200 VDCCs.

introduces delays that are directly correlated to l_c . As already discussed, a synapse with a specific base level release probability can either have a small cluster close by (small l_c) or a large cluster farther off (large l_c). In Fig. 3A, mean delay is plotted as a function of distance for low, high, and medium release probabilities by varying the VDCC cluster sizes at each distance. The synaptic delays were calculated as the time between the peak of the action potential (AP) and mean vesicle release time in a 10-ms window. Closer spatial coupling between the VDCC cluster and the active zone led to faster release. Additionally, the possible range of release probabilities at each distance in the simulation achieved by varying the VDCC cluster size led to a spread in the release times as well. This spread was ~ 1 ms for 10 nm l_c and went up by 50% for 400 nm l_c , implying better precision at smaller l_c . Large calcium influx apart from l_c also had the effect of decreasing delays (compare blue line with red in Fig. 3A).

In Fig. 3B the mean release delays (within 10 ms after AP peak) are given for the entire range of possible release probabilities for VDCC clusters placed between 10 and 400 nm from the active zone, as a function of global peak calcium transient. Thus, we can use the measured synaptic time delay of release and the peak of the global calcium transient to estimate l_c . As long as the apparent diffusion constant of calcium is constrained to be physiologically realistic (26), the l_c calculated from time delays predicted by our model are independent of the precise details of the biophysics of the channels and the kinetic sensor.

Presynaptic Spatial Organization Influences STP. Certain forms of STP, namely facilitation, augmentation, posttetanic potentiation, and depletion are of presynaptic origin and are manifested by modifications to release probability (2, 27). Changes in release probability in an activity-dependent manner plays a prominent role in normal synaptic function (28). Paired-pulse ratio (PPR) is a common protocol for investigating STP.

Because more calcium ions enter synapses with large l_c , limitations on extrusion mechanisms, buffering capacity, and speed augment residual calcium in the presynaptic terminal. If a second stimulus arrives before the excess calcium is extruded, there is an increase in the release probability comprising PPF, as we explored here with simulations.

PPF results observed from a pair of stimuli separated by a 40-ms interval are shown in Fig. 4A (see Fig. S4 for PPF results using a 20-ms interval). Consistent with previous studies (18, 27), greater facilitation was observed in synapses with smaller intrinsic release probabilities for all values of l_c . The narrow range of PPF values at high release probabilities was a consequence of the steep calcium sensitivity response curve (14), saturation at $p_{r1} = 1.0$ and depletion. Here we show that a larger PPF was also associated with larger l_c because of the augmented residual calcium after the first pulse. To get a quantitative understanding of relationship of PPF with l_c , the increase in peak local calcium with large l_c is shown in Fig. 4B. Fig. 4B, *Left Inset* shows the increase in total residual calcium in the presynaptic terminal with increasing l_c as a function of p_{r1} (colored lines, legends indicate l_c in nanometers). This is because more VDCCs are activated at larger l_c (Fig. 4B, *Right Inset*) to reach a threshold of release. The PPF decreased for longer interstimulus intervals (ISIs) (compare Fig. 4A, 40 ms ISI with Fig. S4A, 20 ms ISI) because of the greater decay in residual calcium.

The PPF curves in Fig. 4C are similar to those from experimental data of Dobrunz et al. (27). The mapping between the VDCC cluster size and l_c to the PPF measured at the CA3–CA1 synapses given here determine both l_c and the VDCC cluster size associated with the active zone.

In the structural parameter space (l_c and VDCC number) facilitation is high at large l_c ; this can be clearly seen in our data (Fig. 4C). The typical scale of PPF seen experimentally in CA3–CA1 is 2.5 for 40 ms interpulse interval (Fig. 4C, *Left Inset*) (29). Our model strongly constrains l_c to approximate distances of $300 \text{ nm} \pm 50 \text{ nm}$. Approximately 65 VDCCs placed at 300 nm from the active zone lead to the typical release probability p_{r1} of 20%, typical of CA3–CA1 synapses (18).

Another common way to characterize STP is by separately considering response to the second stimulus in a paired-pulse protocol when the response to the first pulse was a failure (p_{01}) and when response to the first stimulus was a success (p_{11}). If releases are independent events not subject to facilitation or vesicle depletion then one expects that $p_r = p_{r1} = p_{r2}$, therefore $p_{01} = p_r(1 - p_r)$, and $p_{11} = p_r^2$. One possible reason for the second release to be dependent on the first is through depletion

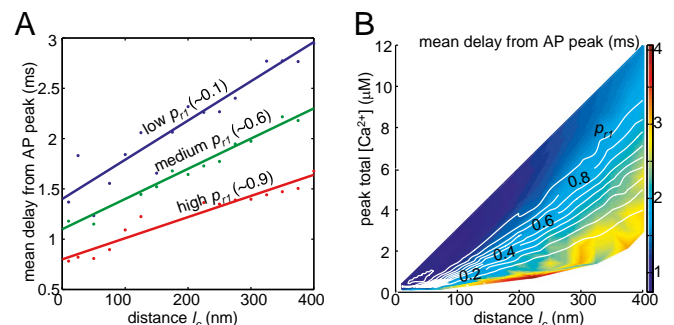
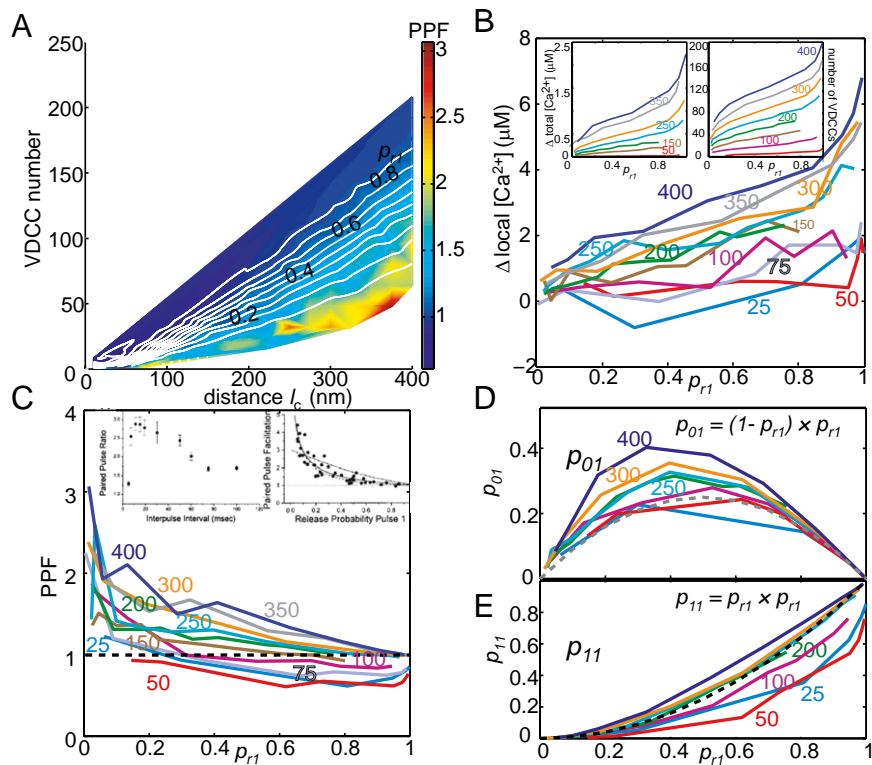


Fig. 3. Using release latencies and peak calcium concentrations to predict l_c . (A) Delays in neurotransmitter release after the arrival of the action potential as a function of various l_c s is shown for a synapse with a low, medium, and high release probability. Release delays were measured for various l_c s and averaged for 1,000 trials in a 10-ms window after the peak of the action potential. (B) Mean release delays (mean over 10 ms and averaged over 1,000 trials) for a range of peak global calcium response and l_c s as predicted by the model. Using this plot and an estimate of release delays, l_c can be deduced.

Fig. 4. Structural correlates of short-term plasticity. (A) Paired-pulse facilitation ratio for a 40-ms interstimulus interval (ISI) protocol as a function of l_c and the VDCC number. Larger facilitation ratios (red) occur for larger l_c and lower release probabilities. (B) Changes in peak of local calcium concentration (local residual calcium), measured 10 nm above the active zone, between first pulse and second pulse (40 ms ISI) as a function of release probabilities, p_{r1} . Legends (color coded) indicate various l_c s in nm. For a given release probability p_{r1} , more calcium channels were activated (VDCCs) for synapses with a larger l_c compared with synapses with shorter l_c (Right Inset). This leads to an increasing residual calcium response with increasing l_c , both local as well as the total calcium (Left Inset). (C) PPF as a function of p_{r1} for a range of l_c (color-coded legends in nanometers). For comparison Left Inset shows PPF averaged over all p_{r1} s for various ISI from Fig. 1B, Dobrunz et al. (29) (see 40 ms ISI data point) and Right Inset shows PPF as a function of p_{r1} for 40 ms ISI from Fig. 3A from Dobrunz et al. (27). Reprinted from *Neuron*, 18, Dobrunz LE, Stevens CF, Heterogeneity of release probability, facilitation, and depletion at central synapses, 995–1008, Copyright (1997) with permission from Elsevier. (D) Probability of vesicle release in response to second stimulus when response to first was a failure (p_{01}). (E) Probability of vesicle release in response to second stimulus when response to first was a success (p_{11}). Dashed lines indicate the phase space in which $p_{01} = (1 - p_{r1}) \times p_{r1}$ (dashed gray) and $p_{11} = p_{r1} \times p_{r1}$ (dashed black), i.e., when both the events are independent. The various l_c s are indicated in color-coded legends (nanometers).



of the RRP. The RRP in CA3–CA1 synapses is a limited resource, approximately seven vesicles on average (30), that takes a few seconds to be replenished after a release event takes place. Given this limited resource and independent vesicle release, one might expect that depletion on its own would give $p_{01} > p_{11}$. On the other hand, given the natural variance of calcium influx, the process of facilitation suggests that having a larger than average calcium response during the first stimulus, as would be expected for a successful initial release, would enhance the second release. This would mitigate and possibly overcome the depletion effect depending on the amount of residual calcium. Fig. 4D shows the expected value of p_{01} [dashed gray curve, $p_{01} = p_r (1 - p_r)$] and Fig. 4E shows p_{11} (dashed black curve, $p_{11} = p_r^2$) with increasing p_{r1} assuming complete independence of release events with no depletion or facilitation (i.e., $p_{r1} = p_{r2}$).

We then measured p_{01} and p_{11} in simulations as we varied the initial release probability, p_{r1} , by varying the number of VDCCs at different values of l_c . In the case of p_{01} there was no depletion because release failed on the first stimulus, and all of the measurements of p_{01} lie above the dashed gray curve, a clear indication of facilitation ($p_{r2} > p_{r1}$) (Fig. 4E). We observed an increasing degree of facilitation with increasing l_c consistent with the interpretation that the observed facilitation was due to increased residual calcium. In the case of p_{11} , depletion occurred due to success of the first stimulus and our measured p_{11} curves for $l_c = 25$ to 100 nm lie below the dashed curve, indicating depression of release probability on the second stimulus ($p_{r2} < p_{r1}$). Taken together with the results for p_{01} , for $l_c = 25$ to 100 nm, this means that the residual calcium from the first stimulus was not enough to overcome the depletion effect for $l_c < \sim 150$ nm. In contrast, our measured p_{11} curves for $l_c = 250$ to 400 nm lie above the dashed curve, indicating that the residual calcium overcame the depletion effect and produced facilitation with $l_c > \sim 150$ nm. Interestingly, our results for p_{11} also show that at $l_c = \sim 200$ nm the effect of depletion and facilitation exactly balance, producing the illusion of independent release probabilities ($p_{r1} = p_{r2}$)

across the entire range of p_{r1} values. Thus, our simulation results reveal the structural information hidden in a relatively simple analysis of release probabilities.

All of the calculations for release and PPF thus far assumed a RRP size of 7 vesicles (30). The major mechanisms involved in short-term plasticity are presynaptic and modulated by changes in release probability (2, 31). The size of the RRP is a significant determinant of the release probability (2, 27). We examine how changes in RRP size affect short-term plasticity in Fig. S5 A–C for RRP sizes of 2, 7, and 25, respectively. The choice of the illustrative RRP sizes span the distribution seen in CA3–CA1 synapses (30). We find that RRP size does not strongly influence PPF across the entire parameter space described by VDCC cluster size and l_c (Fig. S5 A–C and *SI Text*).

Relationship Between Facilitation and Depletion at a Hippocampal Synapse Is an Indicator of the Synaptic Structure. Presynaptic short-term facilitation, and short-term presynaptic depression (STD) (dominated by depletion of neurotransmitter vesicles) are usually assumed to act independently. Facilitation was studied during recovery from depletion caused by hypertonic shock in rodent autaptic hippocampal neurons in cultures. Applying hypertonic solution caused rapid release of vesicles from RRP, whereas the global calcium signal in the presynaptic terminal remained unchanged (32), thus allowing the effects of depletion on short-term facilitation to be investigated. The stimulus consisted of two electrical stimuli separated by 45 ms in a paired-pulse protocol. First, the presynaptic terminal was maximally depleted, then the stimulus was applied, and facilitation to the stimulus recorded at various time points as the synapse slowly recovers from depletion as the docked vesicles returned. The PPF was highest immediately after the application of the hypertonic solution when the synapse was most depleted (Fig. 5, dashed black line). Because it was difficult to estimate the exact size of the RRP at various time points in these in vitro experiments, recovery of releasable vesicles in the RRP was tracked by

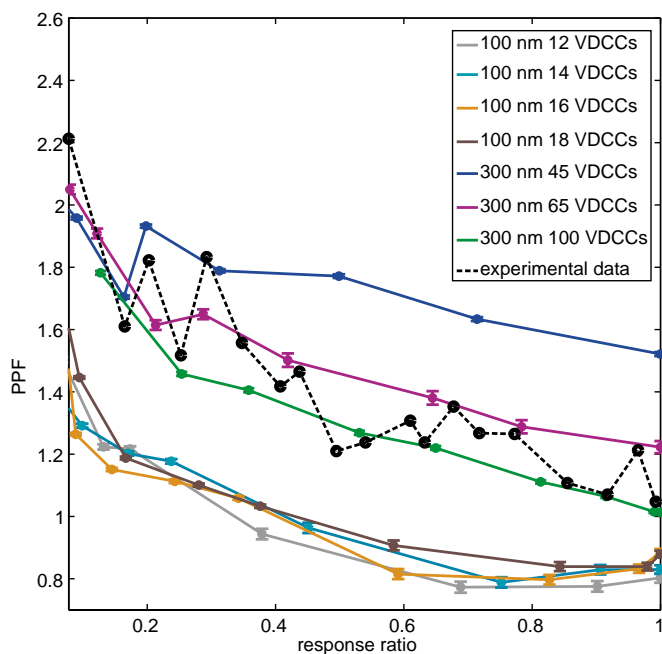


Fig. 5. PPF dependence of response ratio predicts synaptic ultrastructure. Dashed black line shows experimental measurements of PPF (45 ms ISI) as a function of “response ratio,” defined as the fraction of the RRP available during recovery from hypertonic shock. Colored lines indicate the results of simulations carried out with 45 ms ISI with various combinations of l_c and the number of VDCCs. A presynaptic terminal comprising 65–75 VDCCs placed 300 nm away from the active zone best matched the PPF ratio falloff with increasing RRP that is seen in the experimental data.

the “response ratio,” defined as the ratio of the response to the first component of the stimulus posthypertonic shock to the response to the first component of stimulus prehypertonic shock. By definition, the last time point when the synapse completely recovered had a response ratio of 1.0.

We mimicked the experimental protocol of depletion without changing the global calcium response in our computational simulations (in contrast to simulation for different RRP sizes in Fig. S5). We started with a large RRP size of 25 docked vesicles to be consistent with large RRP sizes associated with autaptic synapses in cultures. We then computed the PPF for various RRP sizes (comparable to various stages of recovery from depletion in the experiment) and the corresponding response ratios. Simulation results for a range of structural arrangements are shown in Fig. 5. The structure that best matched the experimental data was composed of a cluster of 65–75 channels at about 300 nm from the active zone and is completely consistent with the previous estimates from PPF data.

Discussion

Using a calibrated model of a CA3–CA1 active zone, we have shown how temporal precision, reliability, and plasticity can all be coordinated by the spatial organization of molecules in the presynaptic terminal. Synapses with low release probabilities facilitate more significantly compared with high release probability synapses (27, 33). This is consistent with our analysis (Fig. 4) of the paired-pulse protocol. We know that the average base level release probability of CA3–CA1 synapses is conspicuously low (20%) providing for an inherently large range over which release response can be varied (27). Separately, we show here that facilitation is high at large l_c ; this can clearly be seen in (Figs. 4A and C and 5). The STP requirements at this synapse as measured with PPF (27, 29) (average PPF of ~ 2.5 for 40 ms ISI), and experimental data in Fig. 5 (dashed black line) constrained the

computational model and yielded a strong prediction for placement of the VDCCs with respect to the docked vesicles.

Our model strongly suggests ~ 65 – 75 calcium channels at an average l_c of ~ 300 nm govern release at the CA3–CA1 synapse. This arrangement leads to an average release probability of $\sim 20\%$, typical for the CA3–CA1 synapse. Similar numbers for l_c and VDCC number per active zone have been estimated at the calyx of Held, a central synapse with hundreds of active zones (10). In contrast, a small number of channels and a spatial nanodomain composed of vesicles and calcium sensors regulate transmitter release in fast GABAergic central neurons (8, 12, 13). GABAergic synapses exhibit a very low PPF and have a high release probability (34) consistent with our simulation results at small l_c , especially at high p_{r1} .

Several experimental studies have considered the response to the second stimulus in a paired-pulse protocol when the response to the first pulse was a success (p_{11}) and when response to the first stimulus was a failure (p_{01}), reaching different conclusions (35–40). Both p_{01} greater than p_{11} (29, 37, 41) and p_{01} to be less than p_{11} (35, 36) have been reported. Activation failure of bouton action potential, depletion, variation in calcium, heterogeneity in the probability of each vesicle release in the RRP, or multivesicular release are some of the reasons cited for the relationship between p_{11} and p_{01} . There is a simpler explanation—the value of intrinsic release probability, p_{r1} .

Our analysis of p_{01} and p_{11} as a function of initial release probability, p_{r1} shows that there are two equally valid regimes with $p_{01} < p_{11}$ as well as $p_{01} > p_{11}$ (Fig. 4D). For low p_{r1} , it is unlikely that a vesicle will be released in response to both the stimuli ($p_{11} < p_{01}$). For high p_{r1} , it is unlikely that a vesicle will “not” be released in response to the first stimuli ($p_{01} < p_{11}$). To set a lower bound on the separation distance, l_c , we plot the contour (black dashed curve) for p_{11} in Fig. 4D in a scenario when the two release events are completely independent, and therefore defined by $p_{r1} = p_{r2}$. All separation distances, l_c , below 200 nm fall below this line immediately providing an insight into the geometrical arrangement. This can be understood again by the interplay between facilitation due to calcium accumulation and depression due to depletion of vesicles. For small separation distances, implying fewer VDCCs governing release, facilitation is limited and depletion rules.

We concluded that the number of VDCCs that govern release in the CA3–CA1 is an order of magnitude greater than the number at GABAergic synapses made by fast spiking interneurons (8). Two independent experimental protocols, one derived from PPF dependence on release probability and the other from PPF dependence upon depletion of the RRP arrived at the same extended geometry. Both datasets were independently fitted and yielded the same high l_c and number of VDCCs. This consistency is reassuring and indicates a unique relationship between structure and function. This is in contrast to GABA and neuromuscular junction synapses, where the VDCCs are close to the calcium sensors, and, may be an adaptation for a highly plastic synapse. It might be possible to locate the VDCCs with the latest advances in superresolution microscopy and to confirm our prediction. The model also makes strong predictions for the variance of calcium concentration in the terminal under different conditions, which could be tested with calcium-sensitive indicators. Furthermore aberration in synaptic function at CA3–CA1 synapses is the source of several neurological diseases. An exploration of mechanisms that affect vesicular release may have important implications for understanding pathological conditions (42).

Methods

Our detailed physical model of the presynaptic terminal implements stochastic reaction–diffusion in a 3D space and incorporates all major sources of variability that can affect vesicle release (43). Simulations were performed using MCell, version 3 (44).

The release dynamics of neurotransmitter at the CA3–CA1 hippocampal synapse and the spatially explicit model of the terminal is discussed in detail elsewhere (14). The model incorporates known details regarding the CA3–CA1 synapse such as the average terminal size (~0.5 μm wide), the number of active zones (typically one), and the typical number of docked vesicles at each active zone (approximately seven). Additionally, it draws on common features of release at central synapses including calcium sensors, multiple time scales, calcium channel kinetics, and buffer kinetics. The kinetic model for release was specifically developed for the CA3–CA1 synapse and is consistent with available data (20, 29, 30, 45, 46).

The major features of the models are a cluster of VDCCs of type P/Q (19, 47) and an active zone populated by seven docked vesicles (30), each endowed with its own (dual) calcium sensor for neurotransmitter release. The detailed kinetics are available in ref. 14 except simulations here were performed with fusion rate for the synchronous sensor, γ set at 6,000 s^{-1} to be consistent with ref. 22 (previous simulations were done with 2,000 s^{-1}). This has no functional consequence; only values of γ , below 1,500 s^{-1} limit the rate of neurotransmitter release. The active zone was placed at a specified separation distance, l_c (center-to-center distance: 25–400 nm) from the VDCC cluster, the source of Ca^{2+} flux (14). This canonical presynaptic terminal was implemented in a rectangular box 0.5 μm wide and 4 μm long representing a segment of an axon making an en passant synapse (14), which is the most common form of synapse in the CA1 neuropil.

We simulated the sequence of events at the CA3–CA1 synapse beginning with the arrival of an action potential (Fig. S1). The arrival of an axonal action

potential depolarizes the presynaptic terminal leading to the stochastic opening of VDCCs. The calcium that enters diffuses from the VDCCs to the calcium sensor, binds to the sensor, and triggers vesicle fusion and glutamate release.

The total calcium flux entering the terminal depended on the time course of the action potential, the number of channels present on the membrane, the calcium conductance of open channels, and the total time each of the channels remains open. The separation distance (l_c) and the VDCC kinetics determine the local calcium profile at the active zone and therefore control the neurotransmitter release probability. Because the simulations are inherently stochastic (see below), we performed 1,000 trials of each test case to generate an average release probability profile for relevant combinations of VDCC number and l_c .

Initial concentrations, locations, diffusion constants, and rates and their sources used in the MCell model are specified in table 1 in ref. 14. The calcium concentration was clamped at 100 nM at both ends of the axon segment. The simulation time step for calcium was 0.1 μs and 1.0 μs for all other molecules. The release transients presented in Fig. S3C were a result of averaging over 10,000 simulations. The docked vesicles were clustered in a hexagonal array at the active zone with largest center-to-center distance between vesicles of 35 nm.

ACKNOWLEDGMENTS. This work was partially supported by the Center for Theoretical Biological Physics (National Science Foundation PHY-0822283); National Institutes of Health Grants MH079076, GM068630, and P01-NS044306; and the Howard Hughes Medical Institute.

- Katz B, Miledi R (1970) Further study of the role of calcium in synaptic transmission. *J Physiol* 207:789–801.
- Zucker RS, Regehr WG (2002) Short-term synaptic plasticity. *Annu Rev Physiol* 64:355–405.
- Lisman JE, Raghavachari S, Tsien RW (2007) The sequence of events that underlie quantal transmission at central glutamatergic synapses. *Nat Rev Neurosci* 8:597–609.
- Augustine GJ, Santamaria F, Tanaka K (2003) Local calcium signaling in neurons. *Neuron* 40:331–346.
- Stanley EF (1997) The calcium channel and the organization of the presynaptic transmitter release face. *Trends Neurosci* 20:404–409.
- Brandt A, Khimich D, Moser T (2005) Few $\text{CaV}1.3$ channels regulate the exocytosis of a synaptic vesicle at the hair cell ribbon synapse. *J Neurosci* 25:11577–11585.
- Shahrezaei V, Cao A, Delaney KR (2006) Ca^{2+} from one or two channels controls fusion of a single vesicle at the frog neuromuscular junction. *J Neurosci* 26:13240–13249.
- Bucurenciu I, Bischofberger J, Jonas P (2010) A small number of open Ca^{2+} channels trigger transmitter release at a central GABAergic synapse. *Nat Neurosci* 13:19–21.
- Mintz IM, Sabatini BL, Regehr WG (1995) Calcium control of transmitter release at a cerebellar synapse. *Neuron* 15:675–688.
- Borst JG, Sakmann B (1996) Calcium influx and transmitter release in a fast CNS synapse. *Nature* 383:431–434.
- Wu LG, Westenbroek RE, Borst JG, Catterall WA, Sakmann B (1999) Calcium channel types with distinct presynaptic localization couple differentially to transmitter release in single calyx-type synapses. *J Neurosci* 19:726–736.
- Bucurenciu I, Kulik A, Schwaller B, Frotscher M, Jonas P (2008) Nanodomain coupling between Ca^{2+} channels and Ca^{2+} sensors promotes fast and efficient transmitter release at a cortical GABAergic synapse. *Neuron* 57:536–545.
- Eggermann E, Bucurenciu I, Goswami SP, Jonas P (2012) Nanodomain coupling between Ca^{2+} channels and sensors of exocytosis at fast mammalian synapses. *Nat Rev Neurosci* 13:7–21.
- Nadkarni S, Bartol TM, Sejnowski TJ, Levine H (2010) Modelling vesicular release at hippocampal synapses. *PLoS Comput Biol* 6:e1000983.
- Coggan JS, et al. (2005) Evidence for ectopic neurotransmission at a neuronal synapse. *Science* 309:446–451.
- Sargent PB, Saviane C, Nielsen TA, DiGregorio DA, Silver RA (2005) Rapid vesicular release, quantal variability, and spillover contribute to the precision and reliability of transmission at a glomerular synapse. *J Neurosci* 25:8173–8187.
- Bertram R, Sherman A, Stanley EF (1996) Single-domain/bound calcium hypothesis of transmitter release and facilitation. *J Neurophysiol* 75:1919–1931.
- Murthy VN, Sejnowski TJ, Stevens CF (1997) Heterogeneous release properties of visualized individual hippocampal synapses. *Neuron* 18:599–612.
- Koester HJ, Sakmann B (2000) Calcium dynamics associated with action potentials in single nerve terminals of pyramidal cells in layer 2/3 of the young rat neocortex. *J Physiol* 529:625–646.
- Goda Y, Stevens CF (1994) Two components of transmitter release at a central synapse. *Proc Natl Acad Sci USA* 91:12942–12946.
- Stevens CF, Sullivan JM (2003) The synaptotagmin C2A domain is part of the calcium sensor controlling fast synaptic transmission. *Neuron* 39:299–308.
- Sun J, et al. (2007) A dual- Ca^{2+} -sensor model for neurotransmitter release in a central synapse. *Nature* 450:676–682.
- Nagy G, Kim J, Pang Z, Matti U (2006) Different effects on fast exocytosis induced by synaptotagmin 1 and 2 isoforms and abundance but not by phosphorylation. *J Neurosci* 26:632–643.
- Xu J, Mashimo T, Südhof TC (2007) Synaptotagmin-1, -2, and -9: Ca^{2+} sensors for fast release that specify distinct presynaptic properties in subsets of neurons. *Neuron* 54:567–581.
- Modchang C, et al. (2010) A comparison of deterministic and stochastic simulations of neuronal vesicle release models. *Phys Biol* 7:026008.
- Allbritton NL, Meyer T, Stryer L (1992) Range of messenger action of calcium ion and inositol 1,4,5-trisphosphate. *Science* 258:1812–1815.
- Dobrunz LE, Stevens CF (1997) Heterogeneity of release probability, facilitation, and depletion at central synapses. *Neuron* 18:995–1008.
- Pfister J-P, Dayan P, Lengyel M (2010) Synapses with short-term plasticity are optimal estimators of presynaptic membrane potentials. *Nat Neurosci* 13:1271–1275.
- Dobrunz LE, Huang EP, Stevens CF (1997) Very short-term plasticity in hippocampal synapses. *Proc Natl Acad Sci USA* 94:14843–14847.
- Murthy VN, Schikorski T, Stevens CF, Zhu Y (2001) Inactivity produces increases in neurotransmitter release and synapse size. *Neuron* 32:673–682.
- Edelman GM, Gall WE, Cowan WM; Neurosciences Institute (1987) *Synaptic Function* (Wiley, New York).
- Rosenmund C, Stevens CF (1996) Definition of the readily releasable pool of vesicles at hippocampal synapses. *Neuron* 16:1197–1207.
- Thomson AM (2000) Facilitation, augmentation and potentiation at central synapses. *Trends Neurosci* 23:305–312.
- Kraushaar U, Jonas P (2000) Efficacy and stability of quantal GABA release at a hippocampal interneuron-principal neuron synapse. *J Neurosci* 20:5594–5607.
- Chen Y, Chad JE, Wheal HV (1996) Synaptic release rather than failure in the conditioning pulse results in paired-pulse facilitation during minimal synaptic stimulation in the rat hippocampal CA1 neurones. *Neurosci Lett* 218:204–208.
- Hanse E, Gustafsson B (2002) Release dependence to a paired stimulus at a synaptic release site with a small variable pool of immediately releasable vesicles. *J Neurosci* 22:4381–4387.
- Hjelmstad GO, Nicoll RA, Malenka RC (1997) Synaptic refractory period provides a measure of probability of release in the hippocampus. *Neuron* 19:1309–1318.
- Isaac JT, Hjelmstad GO, Nicoll RA, Malenka RC (1996) Long-term potentiation at single fiber inputs to hippocampal CA1 pyramidal cells. *Proc Natl Acad Sci USA* 93:8710–8715.
- Stevens CF, Wang Y (1994) Changes in reliability of synaptic function as a mechanism for plasticity. *Nature* 371:704–707.
- Volyanski KE, Rusakov DA, Kullmann DM (2006) Presynaptic fluctuations and release-independent depression. *Nat Neurosci* 9:1091–1093.
- Thomson AM, Bannister AP (1999) Release-independent depression at pyramidal inputs onto specific cell targets: Dual recordings in slices of rat cortex. *J Physiol* 519:57–70.
- Zhang C, et al. (2009) Presenilins are essential for regulating neurotransmitter release. *Nature* 460:632–636.
- Ribault C, Sekimoto K, Triller A (2011) From the stochasticity of molecular processes to the variability of synaptic transmission. *Nat Rev Neurosci* 12:375–387.
- Kerr RA, et al. (2008) Fast Monte Carlo simulation methods for biological reaction-diffusion systems in solution and on surfaces. *SIAM J Sci Comput* 30:3126.
- Dodge FA, Jr., Rahamimoff R (1967) Co-operative action of calcium ions in transmitter release at the neuromuscular junction. *J Physiol* 193:419–432.
- Otsu Y, Murphy TH (2003) Miniature transmitter release: Accident of nature or careful design? *Sci STKE* 2003:pe54.
- Reid CA, Bekkers JM, Clements JD (2003) Presynaptic Ca^{2+} channels: A functional patchwork. *Trends Neurosci* 26:683–687.

Supporting Information

Nadkarni et al. 10.1073/pnas.1211971109

SI Text

In Fig. S5, we show the release probability for the second stimulus as a function of release probability for the first stimulus, for RRP sizes of 2, 7, and 25, respectively. Comparing *A*, *B*, and *C* of Fig. 5, the RRP size does not strongly influence PPF across the entire parameter space described by voltage-dependent calcium channel (VDCC) cluster size and l_c . To emphasize this somewhat surprising result, we take a cross-section at $p_{r1} = 0.5$ for each RRP size and plot it in Fig. S5D. The error bars for p_{r2} at each distance overlap for the RRP sizes with 7 and 25 vesicles and the curve for RRP of 2 has only a relatively minor reduction. This implies a significant robustness of PPF with respect to RRP size.

Although the facilitation is relatively insensitive to RRP size, there is clearly a depletion effect that gets worse as the RRP gets smaller, so there must be a compensating feature. To understand this, for any value of total release probability of the synapse, the release probability per vesicle goes down as RRP goes up. This reduction reduces the expected facilitation, because less calcium is needed to stimulate release and hence there is less residual calcium. This partial compensation works better at larger distances (where there is more residual calcium) and indeed the data in Fig. S5D indicate that an RRP of 7 gives a facilitation below that of an RRP of 25 for the shortest distances. Because the extreme RRP of 2 is dominated by depletion, it always falls below the other cases.

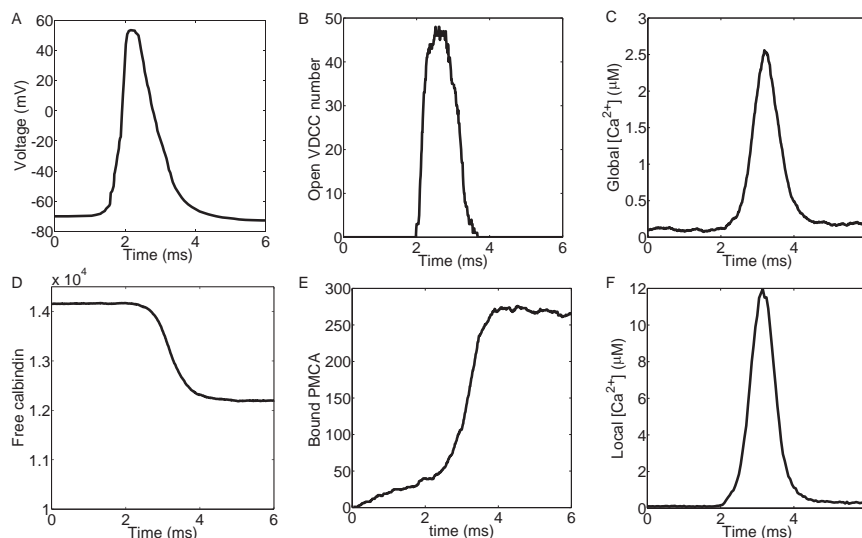


Fig. S1. Chronological sequence of events preceding vesicle release for a typical synapse with 20% release probability. (A) Profile of an action potential invading the terminal of a synapse with 48 VDCCs placed 250 nm from the active zone. (B) Number of open calcium channels in response to the action potential in A. (C) Approximately 4,000 calcium ions entered the presynaptic terminal (70–80 ions per channel). (D) The incoming calcium quickly bound to the mobile calcium buffer, decreasing the amount of free calbindin. (E) The entering calcium increased the plasma membrane calcium ATPase (PMCA) activity. (F) The local calcium signal measured 10 nm above the active zone as a result of the opening of 48 channels placed 250 nm from the active zone.

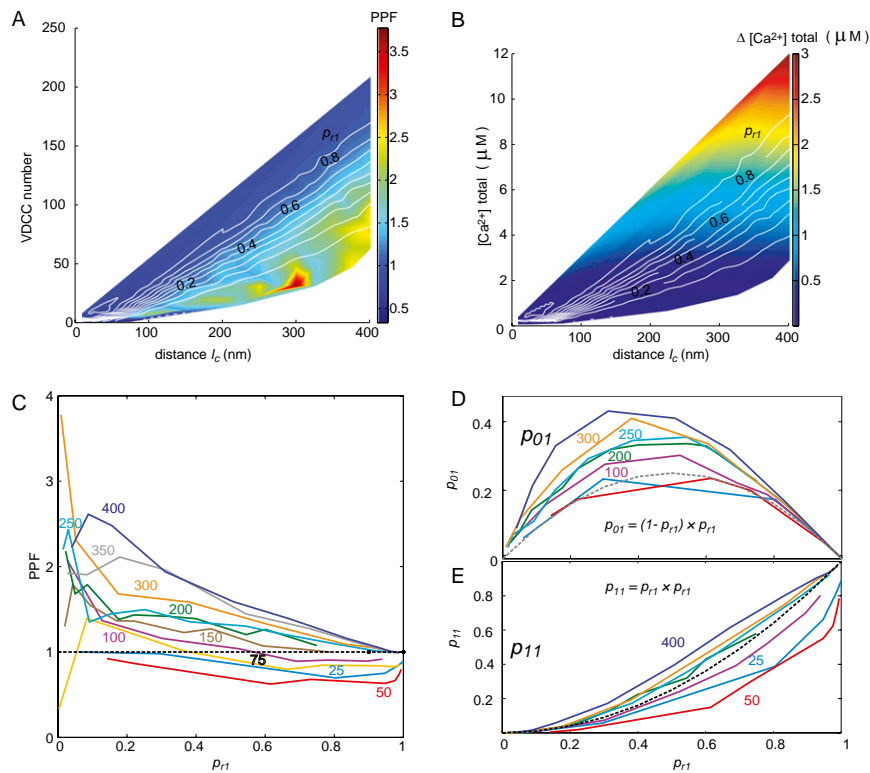


Fig. 54. Structural correlates of short-term plasticity, ISI 20 ms. (A) Paired-pulse facilitation ratio for a 20 ms interstimulus interval (ISI) protocol as a function of l_c and the VDCC number. Larger facilitation ratios (red) occur for larger l_c and lower release probabilities. (B) Changes in peak of total calcium concentration (residual calcium concentration) between first pulse and second pulse (20 ms ISI) as a function of total calcium concentration and l_c . Legends indicate various p_{r1} . (C) PPF as a function of p_{r1} for a range of l_c . The various l_c s are indicated in color-coded legends (nanometers). For synapses with large release probabilities, vesicle depletion offsets the facilitation induced by increased residual calcium at large distances. (D) Probability of vesicle release in response to second stimulus when response to first was a failure (p_{01}). (E) Probability of vesicle release in response to second stimulus when response to first was a success (p_{11}). Dashed lines indicate the phase space in which $p_{01} = (1 - p_{r1}) \times p_{r1}$ (dashed gray) and $p_{11} = p_{r1} \times p_{r1}$ (dashed black), i.e., when both the events are independent. The various l_c s are indicated in color-coded legends (nanometers).

